Nano Energy 41 (2017) 511–518

Contents lists available at ScienceDirect

Nano Energy

journal homepage: www.elsevier.com/locate/nanoen

Full paper

A stretchable fiber nanogenerator for versatile mechanical energy harvesting and self-powered full-range personal healthcare monitoring

Yin Cheng[a], Xin Lu[a], Kwok Hoe Chan[a], Ranran Wang[b], Zherui Cao[b], Jing Sun[b], Ghim Wei Ho[a,*]

[a] Department of Electrical and Computer Engineering, National University of Singapore, 4 Engineering Drive 3, Singapore 117583, Singapore

[b] State Key Laboratory of High Performance Ceramics and Superfine Microstructure, Shanghai Institute of Ceramics, Chinese Academy of Sciences, Shanghai 200050, China

ARTICLE INFO

Keywords:
Stretchable fiber nanogenerator
Wearable
Self-powered
Personal healthcare monitoring

ABSTRACT

Wearable electronics have gained dramatic development in recent years, owing to the advancement in flexible/stretchable electronics, and achieved considerable progress in various applications. Nanogenerators capable of harvesting energy from human activities is considered as a promising alternative for powering the wearable electronic devices, considering the sustainability and rich biomechanical energy from human body. Currently, most of the nanogenerators are aimed at converting limited forms of mechanical energy, mostly pressing or bending, which hampers adaptive exploitation of bodily energy source. Also, the incapability to respond to multiple forms of mechanical stimuli deters the nanogenerators from functioning as full-range human activities sensors. Here, we devise a stretchable integrated nanogenerator-sensory coaxial core-sheath fiber with improved functionality and sustainability. The combination of materials engineering and structure design enables the fiber to scavenge versatile mechanical energy, including stretch, bend, twist and press, through a gap size variation induced electrostatic effect. Besides, the fiber realizes the detection of joint-bending and joint-twisting related motions, such as walking and elbow rotation, and also succeeds in capturing subtle physiological signals, such as breath, pulse and speech recognition, which paves the way for full-range personal healthcare monitoring and documenting in a self-powered, wearable and noninvasive manner.

1. Introduction

Wearable electronics has attracted intensive research interest and, fueled by the advance in flexible and stretchable electronics [1–5], also achieved considerable progress in various applications such as healthcare monitoring [6–12], smart prosthetics [13–15], and human-machine interaction [12,16,17]. Typically these wearable devices require external power supplies. Considering the device compactness and sustainability (no need for battery replacement or periodic charging), it is highly desired to integrate a power generator capable of scavenging energy from ambient environment. As human body represents a notably abundant source of biomechanical energy in daily life [18–20], a series of generator devices have been developed to couple energy harvesting with various human activities, based on multiple mechanisms including the piezoelectric effect [21–24], the triboelectric effect [8,25–29], and the electrostatic effect [30–32]. Nevertheless, the vast majority of these generators are aimed at converting limited forms of mechanical energy, mostly pressing [27,33–35] or bending [21,22,36,37], due to the restrictions imposed by component materials or device structure. Thus, the efficient exploitation of biomechanical energy is inevitably confined in view of its diversified forms derived from complex human activities, specifically, stretch, bend, twist and press. On the other hand, some researchers have employed wearable generators in self-powered human activities sensing. Although quite a few fascinating results are demonstrated, currently these self-powered sensing devices are typically targeted at a single type of human activities, such as vigorous human motions [8,37–40] or subtle physiological signals [34,41–44]. Again, this sensing performance deficiency stems from the incapability of the generators to respond to multiple forms of mechanical stimuli, and also the limited sensing range to a specific deformation form, such as tensile strain and pressure. With these concerns in mind, a wearable generator for capturing multiple forms of mechanical energy is particularly desirable and yet remains a great challenge.

Compared with film-structured devices, fiber nanogenerators possess conspicuous advantages of lightweightness, flexibility, compactness and wearing comfort. Xu et al. [45] reported a copper wire-convolving fiber as stretchable nanogenerator, and succeeded in harvesting stretching-mode mechanical energy up to strain of 70%. Zhong et al. [46] developed a stretchable fiber nanogenerator with PTFE and CNT electrodes twining around silicone fiber, and this fiber nanogenerator

* Corresponding author.
E-mail address: elehgw@nus.edu.sg (G. Wei Ho).

http://dx.doi.org/10.1016/j.nanoen.2017.10.010
Received 25 July 2017; Received in revised form 22 September 2017; Accepted 2 October 2017
Available online 05 October 2017
2211-2855/

could serve as sensor of strain up to 25%. Sim et al. [47] introduced a PVDF-TrFE based stretchable triboelectric nanogenerator, with the ability of converting mechanical energy of stretching mode up to strain of 50% to electricity. However, none of the above fiber nanogenerators have exhibited the capability of energy harvesting in stretching, bending, twisting and pressing modes simultaneously. Also, only very limited report [40] has realized the detection of both vigorous motions and subtle physiological signals.

Here we achieve such a stretchable nanogenerator (NG) with a coaxial core-sheath fiber architecture. This fiber nanogenerator (FNG) effectively produces microstructure variation in response to a variety of mechanical stimuli, including stretch, bend, twist and press, owing to the combination of deliberate materials engineering (the core and sheath electrodes) and rational configuration design (coaxial fiber with air gap). Through the electrostatic effect, the microstructure variation (mechanical energy) is converted into electric power, with a maximum peak power density of 2.25 nW/cm^2 and reliable durability (4000 testing cycles). Furthermore, the versatile mechanical stimuli responsive ability of the FNG is harnessed to realize the detection of human activities ranging from vigorous motions such as finger bending, walking, and forearm rotation, to subtle physiological signals like pulse, respiration, and throat-related activities. Such a self-powered full-range wearable fiber holds great application potential in personal healthcare monitoring.

2. Results & discussion

2.1. Design concept and working mechanism of the FNG

Fig. 1a shows the schematic illustration of the FNG structure, featuring a coaxial fiber configuration. The FNG was assembled from a core fiber comprising Ag nanowire (AgNW) and polytetrafluoroethylene (PTFE) coatings on a bare polyurethane (PU) fiber, and a sheath electrode of polydimethylsiloxane-AgNW (PDMS-AgNW) film. An air gap was introduced in between the core fiber and the sheath. The as-prepared FNG is adequately flexible to conform to arbitrarily curved surfaces, such as human finger (Fig. 1b, left), and also highly stretchable (Fig. 1b, right). To understand the working mechanism, the FNG was simplified into an equivalent circuit model with an external load of R as in Fig. 1c-e. Originally, the surface of the PTFE layer was negatively charged by plasma polarization, while the sheath electrode was grounded (Fig. 1c). Simultaneously the PU-AgNW layer of the core fiber and the PDMS-AgNW layer of the sheath electrode were positively charged due to the electrostatic induction and conservation of charge [30,46]. No electrical potential difference between the PU-AgNW and PDMS-AgNW layers existed at the initial equilibrium state. When the outer mechanical stimuli forced the air gap to shrink (Fig. 1d), the PDMS-AgNW layer would produce more positive charges due to enhanced electrostatic induction, thus generating an electric potential difference across the two mentioned layers. To balance the potential difference, free electrons would flow from the PDMS-AgNW layer to the PU-AgNW layer and then reach a new equilibrium. When the air gap reverted to the original state after the release of the mechanical stimuli (Fig. 1e), similarly the equilibrium was broken again and free electrons would flow back from the PU-AgNW layer to the PDMS-AgNW layer. In this way, an alternate current was generated across the external load R, indicating that the mechanical energy involved in the gap size variation was converted into electrical power. This gap size variation induced electrostatic effect differs from the extensively studied triboelectric nanogenerator in the charge generation, instead of triboelectrification, the PTFE as electret material is first charged through plasma polarization.

2.2. Fabrication and characterization of the FNG

Fig. 2a presents the scanning electron microscope (SEM) image of the bare PU fiber (diameter of 650 μm), which serves as a highly flexible and stretchable (ultimate tensile strain up to 1000%, see stress-strain curve in Fig. S1) scaffold of the core fiber. Through a facile press-and-roll method (detailed fabrication process in Experimental Section and Fig. S2 in Supporting information), AgNW film was transferred from silicon substrate onto the surface of the PU fiber to form a homogeneous PU-AgNW composite layer (thickness of ~ 15 μm, cross-section SEM image in Fig. S3, elemental mapping in Fig. S4). The PU fiber was prestretched before AgNW transfer and then released, in order to form buckling microstructure on the surface. The prestretch strain was optimized to be 100% to obtain a distinct buckling (Fig. 2b and the inset) without severe cracking caused by radial expansion along with prestrain release. Detailed SEM characterization results of the PU-AgNW fibers for different prestrain are shown in Fig. S5. The buckling microstructure not only promotes the electromechanical stability of the PU-AgNW as a flexible fiber electrode [48–50], but also facilitates the efficient coating of the PTFE by virtue of the anchoring effect from the remarkably enhanced surface roughness. As seen in Fig. 2c, a uniform PTFE layer (thickness of ~ 30 μm, cross-section and high-magnification surface SEM characterization in Fig. S6) was coated onto the PU-AgNW surface (detailed fabrication process in Experimental Section in Supporting information). The PU-AgNW-PTFE core fiber could be bent to a small radius of curvature (2.6 mm, Fig. S7) without observable delamination of the PTFE layer (inset in Fig. 2c), exhibiting excellent flexibility inherited from the PU fiber. The sheath electrode was prepared through an in-situ polymerization and transfer method (detailed fabrication process in Experimental Section and Fig. S8 in Supporting information). Briefly, AgNW percolation network was formed on a silicon substrate and went through annealing treatment to enable the nanowelding of the AgNW network (marked by circles in Fig. 2d, more information in Fig. S9), which improves both the electric conductivity (Fig. S10) and structural robustness against mechanical impact (Fig. S11) [51–53]. The thermal annealing can not only remove the solvent and organic residues (polyvinyl pyrrolidone as disperse agent of AgNW)

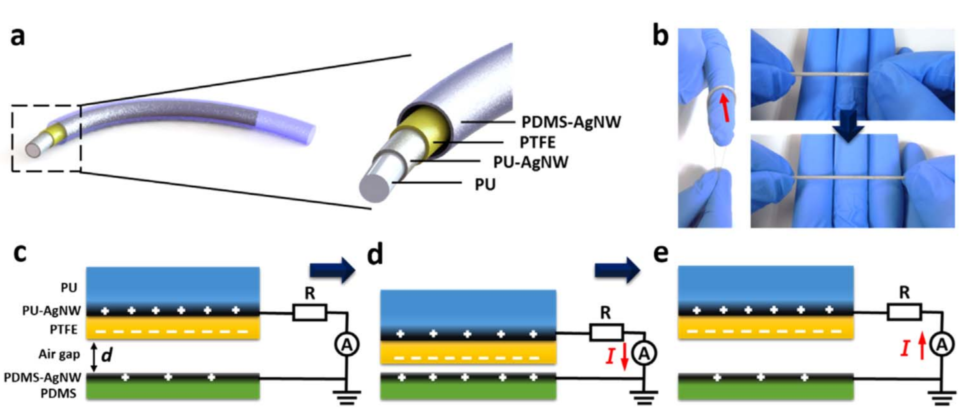

Fig. 1. Schematic illustrations of the FNG structure and the operation mechanism. (a) The structural schematic diagram of the FNG device. The external electric circuiting is omitted for clarity. (b) The photograph of the FNG device wrapping around a finger (marked by the red arrow, left) and being stretched to strain of ~ 50% (right). (c-e) The operation mechanism illustration including a cycle of gap size decrease and recover.

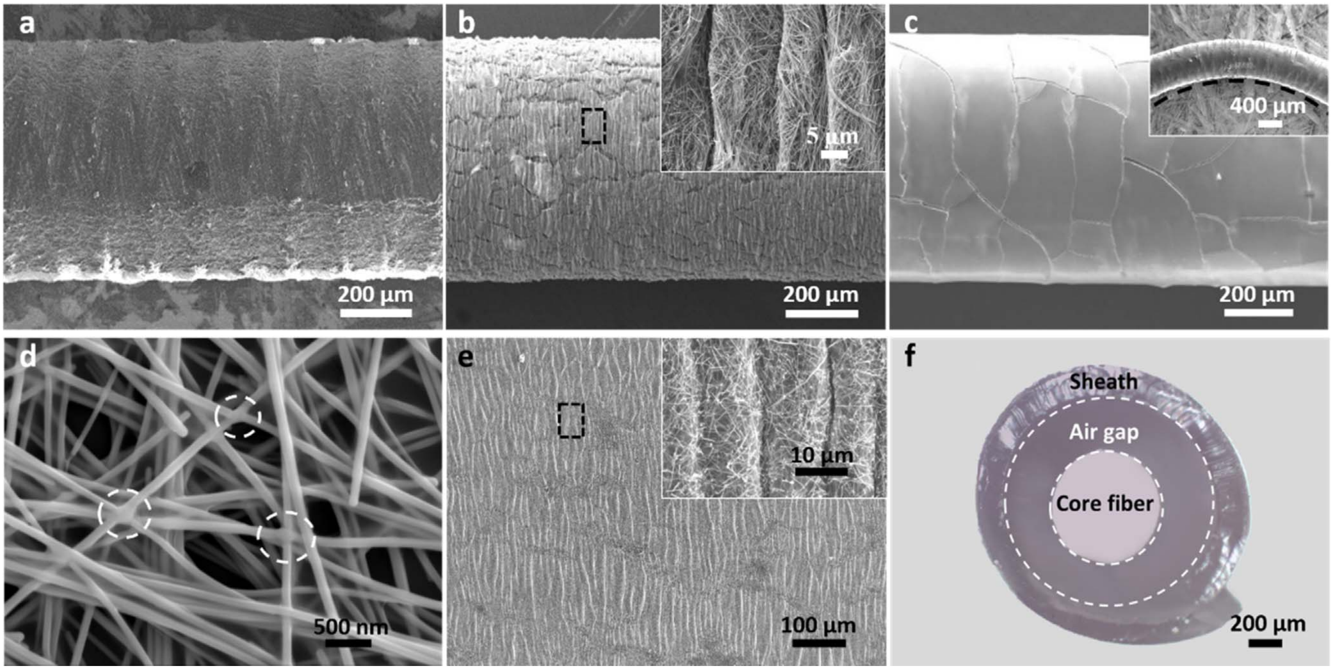

Fig. 2. The characterization of the component materials of FNG. (a) SEM image of the bare PU fiber. (b) SEM image of the PU-AgNW fiber (prestrain of 100%) and the enlarged view of the black dotted box (inset). (c) SEM image of the PU-AgNW-PTFE core fiber. The inset shows the bending state of the core fiber. (d) SEM image of the AgNW network after annealing, white dotted circles mark the nanowelding junctions. (e) SEM image of the PDMS-AgNW film and the enlarged view of the black dotted box (inset). (f) Optic image of the cross-sectional structure of the FNG. The air gap region between the core fiber and the sheath is marked out by white dotted circles.

on the AgNW network, but also enable the enhanced atomic mobility and diffusion for localized nanowelding at contact positions of adjacent nanowires. Then, a prestretched PDMS film was attached on the AgNW network intimately, with liquid PDMS in between as binding layer. After the curing of the binding layer, the AgNW network was successfully transferred to the PDMS surface in the form of a PDMS-AgNW composite layer (thickness of ~ 5 μm, cross-sectional SEM image in Fig. S12). As the prestrain of the PDMS film was released, similarly, an out-of-plane buckling microstructure in the PDMS-AgNW layer was constructed spontaneously (Fig. 2d and inset), which was critically important for improved electromechanical performance as a stretchable electrode (discussed in the next part). The core fiber and the PDMS-AgNW film were integrated into the FNG device (see detailed assembly process in Experimental Section in Supporting information). Fig. 2f displays the optical microscope (OM) image of the cross-section of the FNG device, clearly showing the coaxial fiber configuration (device diameter of ~1.6 mm) with an air gap of ~250 μm sandwiched between a core fiber of PU-AgNW-PTFE and a sheath electrode of PDMS-

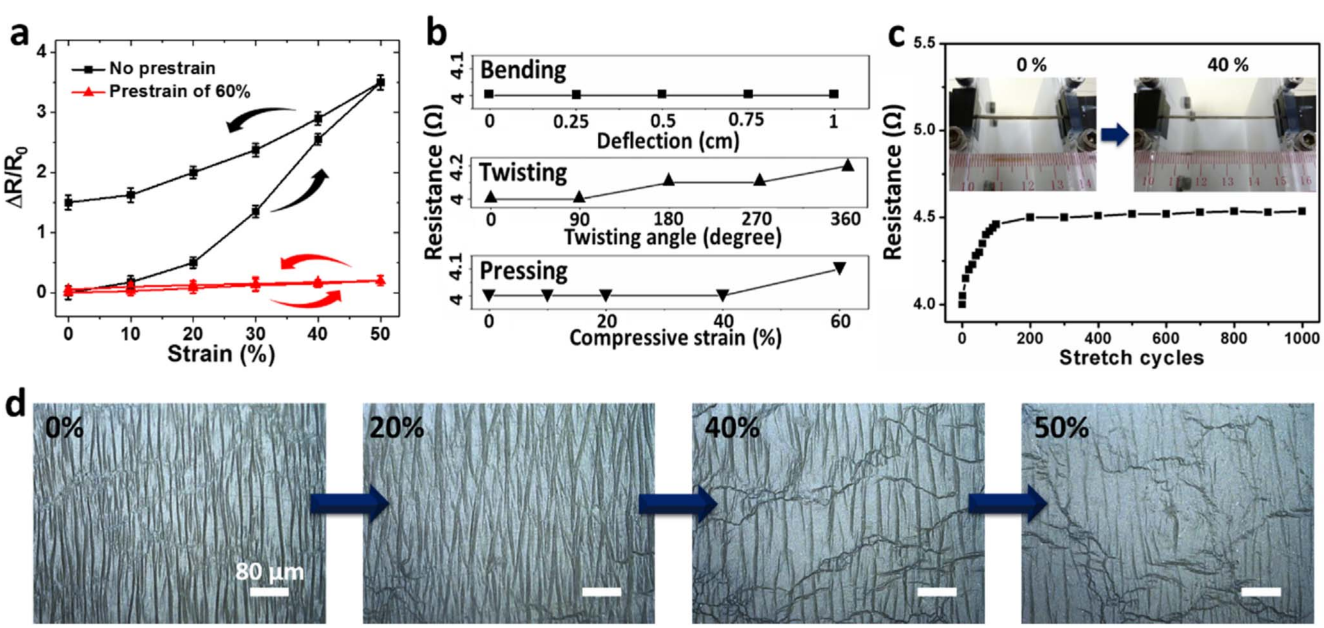

Fig. 3. Characterization of electromechanical properties of the sheath electrode. (a) The relative resistance variation of the sheath electrodes with no prestrain and prestrain of 60%, within a stretch-release cycle of 50% tensile strain. (b) The resistance variation of the sheath electrode (prestrain of 60%) under bending, twisting and pressing test. (c) Resistance variation of the sheath electrode (prestrain of 60%) though cyclic stretching test (strain of 40%). The insets show the photographs of the sheath electrode at original state and stretched state. (d) The surface morphology (AgNW-PDMS side) variation of the sheath electrode with prestrain of 60% during stretching up to strain of 50%.

AgNW (thickness of ~ 200 μm).

2.3. Electromechanical properties of the sheath electrode

During working of the FNG, the sheath electrode underwent various kinds of mechanical impacts, like stretch, bend, twisting and press. Apparently, to ensure the normal operation of the FNG, it is an essential prerequisite for the sheath electrode to maintain a stable electric conductivity while subjected to frequent mechanical impacts. The electromechanical properties of the sheath electrode (length of 4 cm, initial resistance of 4 Ω) were investigated through comprehensive tests. Fig. 3a reveals the relative resistance variation of a sheath electrode with prestrain of 60% during fabrication, and also that of sheath electrode without prestrain as comparison. The resistance of the sheath electrode without prestrain keeps increasing monotonically along with the tensile strain, by 3.5 times at strain of 50%, and retains a residual resistance increase of 150% even though the stretch was completely released. In stark contrast, the sheath electrode holds a remarkably stable resistance across the whole stretch-release cycle within strain of 50%. To illuminate the mechanism underlying the performance difference, the surface microstructures of both the above sheath electrodes were traced via OM characterization. For the sheath electrode without prestrain, microcracks occurred at strain of 10% and propagated at larger strains, suggesting permanent damage to the PDMS-AgNW layer (OM images in Fig. S13). For the sheath electrode with prestrain of 60% (Fig. 3d), the initially buckled PDMS-AgNW layer spread out gradually into a flat surface, thus effectively accommodating the loaded strain without obvious effect to the AgNW percolation network. Similar buckling methods have been presented before and proved to be a valid strategy to prepare stretchable electrodes [54–56]. The sheath electrode with prestrain of 60% (length of 4 cm, initial resistance of 4 Ω) was chosen for the following investigation, unless otherwise specified. Next, other forms of mechanical impacts loading tests were implemented to evaluate the electromechanical properties of the sheath electrode. As seen in Fig. 3b, the electric conductivity of the sheath electrode remained exceedingly stable during the bending (deflection up to 1 cm), twisting (twisting angle up to 360°), and pressing (compressive strain up to 60%), with a negligible resistance increase of within 5%. This mechanical robustness of sheath electrode is probably attributed to the combination of the protection supported by the bonding of AgNW network with polymer matrix and the reinforced mechanical robustness of the AgNW percolation network imparted by the nanowelding effect aforementioned. Lastly, the durability and reliability was assessed by cyclic stretching test at strain of 40%. Fig. 3c displays the resistance variation of the sheath electrode after specified stretching cycles: the resistance went through a small increase from 4 to 4.5 Ω within the first one hundred cycles, and then plateaued, even up to 1000 cycles. Besides, cyclic bending, twisting and pressing tests all revealed reliable

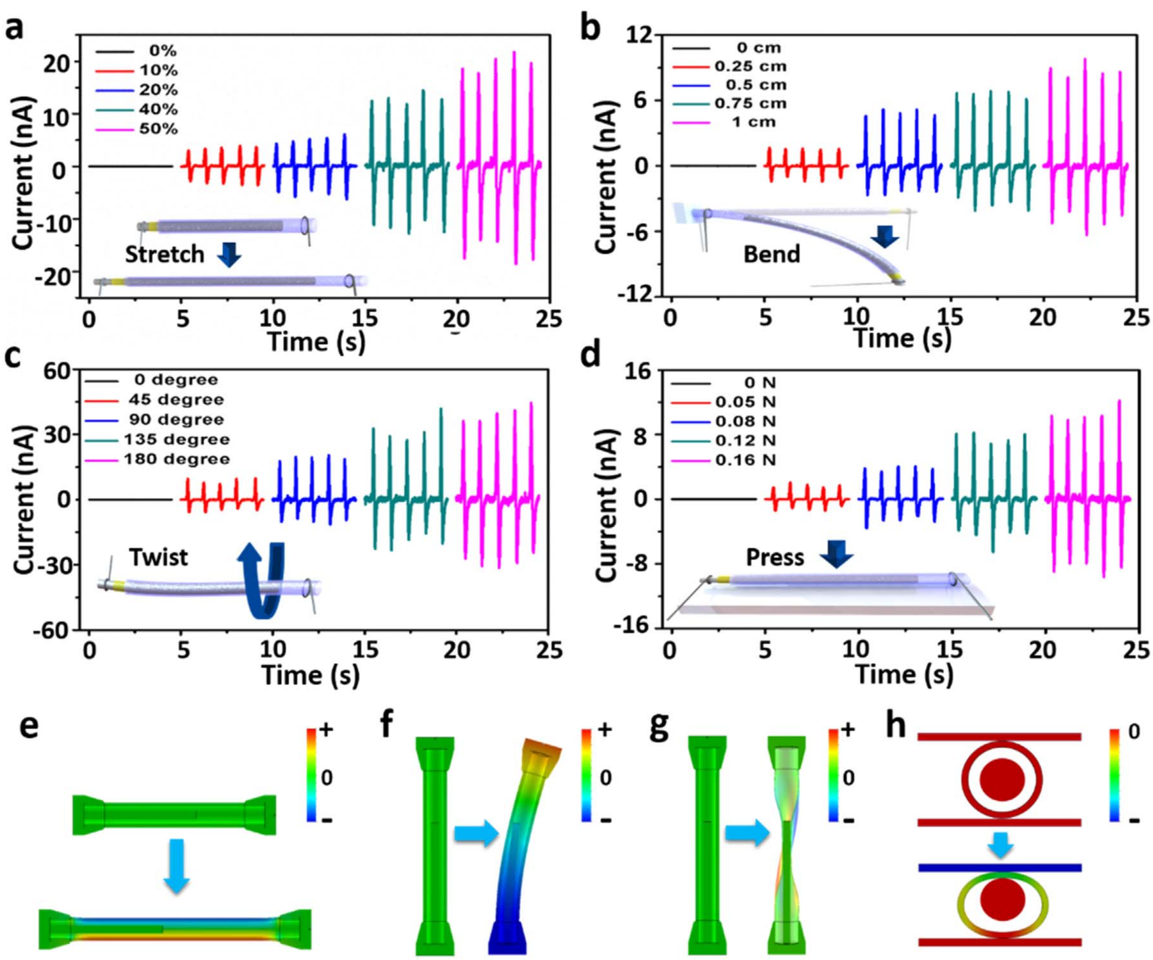

Fig. 4. Versatile mechanical energy conversion properties of the FNG and the mechanical simulation of the structural response to different mechanical stimuli. (a-d) The output short-circuit current of the FNG under mechanical input of stretching (strain of 0–50%), bending (deflection of 0–1 cm), twisting (angle of 0–180°) and pressing (force of 0–0.16 N). The insets in a-d) depicted the illustrations of the FNG device under different mechanical stimuli. (e-h) Simulation results shows the position change of the sheath electrode relative to the axial of the FNG, i.e., the core fiber. (e) For stretching (tensile strain of 50%), define upward displacement relative to the core fiber as positive, the downward as negative. (f) For bending (deflection of 0.8 cm), define rightward displacement relative to the core fiber as positive, leftward as negative. (g) For twisting (twisting angle of 270°), define rightward displacement relative to the core fiber as positive, leftward as negative. (h) For pressing (compressive strain of 15%), define downward displacement relative to the core fiber as negative, upward as positive.

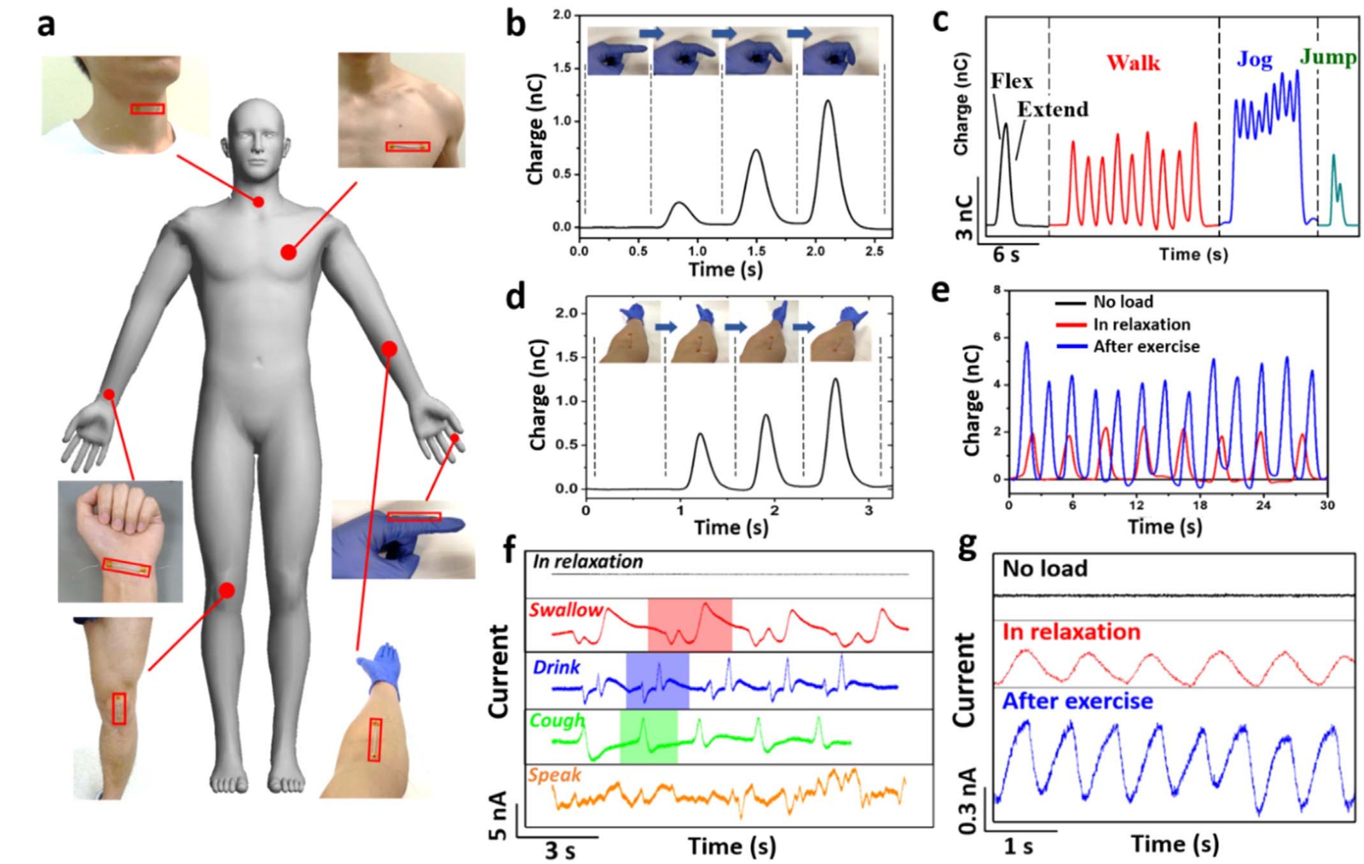

Fig. 5. The wearable self-powered healthcare monitoring application of the FNG. (a) Schematic illustration of the FNG as wearable sensor attached onto different positions of human body, including knuckle and knee for joint-bending related motions, elbow for joint-twisting related motions, and chest/throat/wrist for physiological signals. (b) Finger bending monitoring: charge curve of the FNG (knuckle position) in response to finger bending to increasing degree (shown in inset). (c) Knee-related motions monitoring: charge curve of the FNG (knee position) in response to knee flexing/extending, walking, jogging, and jumping. (d) Elbow twisting monitoring: charge curve of the FNG (elbow position) in response to twisting the forearm to increasing degree (shown in inset). (e) Respiration monitoring: charge curve of the FNG (chest position) in response to respiration before wearing, in relaxation and after exercise. (f) Throat-related activities monitoring: output current of the FNG (throat position) in relaxation and in response to saliva swallow, water drinking, cough, and speaking. The signature waveforms for saliva swallow, water drinking and cough were marked by colored shadows. (g) Pulse monitoring: output current of the FNG (wrist position) before wearing, in relaxation, and after exercise.

electromechanical stability: the resistance increase was within 12% after 1000 testing cycles (Fig. S14 in Supporting information). The superb durability attests to highly qualified deformable electrode for the FNG.

2.4. Versatile mechanical energy harvesting of the FNG

The electricity generation properties of the FNG (4 cm in length) were tested under different mechanical stimuli types. Fig. 4a-d record the output short-circuit currents of the FNG when periodic (frequency of 1 Hz) stretch, bend, twist and press were input (illustrations shown in the insets, Movie S1, Supporting information). In Fig. 4a, as the stretch strain increased from 10% to 50%, the output currents increased from 1.5 to 20 nA, correspondingly. Similarly, the output currents raised along with the increased deformation extent, with the current value being 9, 35, 10 nA, at maximum deforming extent of 1 cm deflection for bending (Fig. 4b), 180° for twisting (Fig. 4c), and 0.16 N for pressing (Fig. 4d), respectively. Note that frequent stretching (tens of cycles) of strain above 50% might rupture the sheath electrode, and larger degree of bending, twisting and pressing led to no noticeable increase of output current. The capability of capturing mechanical energy with various deformation forms benefits not only the efficient energy harvesting, but also the broadened personal healthcare monitoring (see Table S1 for detailed comparison with other reported works). In order to confirm the current generation from the FNG, switching polarity test (detailed information in Fig. S15) was carried out and the results verified the measured output signal came from the FNG rather than the measurement system. To evaluate the level of the output power density of the FNG, periodic twisting (frequency of 1 Hz, twisting angle of 135°) was applied and output performance was recorded under varying external loads (Fig. S16). The load peak voltage increased from 0.13 V at 6 MΩ to 0.66 V at 100 MΩ, and then saturated at the open-circuit voltage. The peak current exhibited a reversed tendency, decreasing from 15 to 1 nA at the same external loads. Accordingly, the maximum output power density was determined to be 2.25 nW/cm^2 at an optimal load of 50 MΩ. Furthermore, the durability of the FNG device was tested by applying ~ 4000 stretching-releasing cycles (strain of 40%) and the output short-circuit current proved to be quite stable after an initial decrease (Fig. S17). The cyclic bending, twisting and pressing tests also revealed quite stable performance (Fig. S18), indicating the reliability for long-term application. For further understanding the electricity generation mechanism, the structural response of the FNG to various mechanical stimuli (Fig. 4e-h) was simulated to analyze the corresponding gap size variation, by using *Solid Works* (see details in Experimental Section in Supporting Information). Fig. 4e and Fig. 4g verifies stretching and twisting decrease the gap size around the core fiber, thus generating electric power. For the cases of bending (Fig. 4f) and pressing (Fig. 4h), the gap around the core fiber involves both size decrease and increase areas: For bending, the gap on the left of the core fiber shrinks and the right part expands; for pressing, the gap vertically shrinks and horizontally expands. We speculate it is the approximately exponential dependence of the charge density of the electrodes on the gap size that led to a net current in the external circuit [31,57]. The simulation results agree well with the testing data: the output current under twisting is much higher than those under other mechanical stimuli (Fig. 4a-d), as the twisting causes much higher level of gap size shrinkage than other cases (Fig. 4e-h).

Supplementary material related to this article can be found online at http://dx.doi.org/10.1016/j.nanoen.2017.10.010.

2.5. FNG as self-powered, wearable sensors for full-range personal healthcare monitoring

Equipped with the high sensitivity to versatile mechanical deformations and the exceptional features including light-weighted (~ 0.04 g/cm), stretchable, biocompatible (packaging material of PDMS), and non-invasive, the FNG is especially well-suited for wearable self-powered monitoring of various human activities and physiological signals. The FNG is directly attached onto a series of body positions for associated detection of personal activities (as seen in Fig. 5a). Firstly, most of human movements are related to joint bending, accompanied by strain variation of surrounding skin. Through the stretch/bend sensing mode of the FNG, the joint-bending related motions can be effectively sensed. Fig. 5b displays the charge curve of the FNG (attached onto the knuckle), which precisely reflects the movements of the wearer bending the finger forward and backward consecutively with three increasing angles (inset in Fig. 5b). Here we adopt the charge curve analysis (the time integral of current) as the charge accumulation is determined directly and exclusively by the gap size variation, thus it is more suitable especially when tracking of the whole motion process is desired (detailed information in Note S1) [30,46]. In Fig. 5c, the FNG sensor (attached onto knee position) records the charge curve of knee-related motions, and can discriminate various motions including knee flexing/extending, walking, jogging, and jumping, according to their distinctly differentiated waveforms. Secondly, joint twisting is another important motion type, which can be detected by means of the twist sensing mode of the FNG. In Fig. 5d, the charge curve of the FNG (attached onto the elbow position across the upper and lower arm) shows the rotation of the forearm with increasing twist angles (inset in Fig. 5d) clearly. The monitoring of such above human movements holds extensive application prospects in sports training and physical rehabilitation for elderly and infirmed persons [58–60]. Thirdly, human physiological activities typically involve mechanical output of pressure, like breathing, phonation, and pulse. The FNG succeeds in capturing these subtle physiological signals via the press sensing mode, by virtue of its low triggering force in pressure sensing (Note S2). Respiration is a vital signal of great significance. When attached onto the chest, the FNG allows real-time recording of the respiration rate and depth through the frequency and magnitude of the peaks of the charge curve, both in relaxation and after exercise (Fig. 5e). This respiration detection not only provides rich information about the functioning of cardiorespiratory system, but also serves as early warning system for sudden infant death syndrome and sleep apnea in adults [61,62]. Fig. 5f depicts the output current of the FNG (attached onto the throat position) during continuous throat-related activities. Each specific activity, including saliva swallow, water drinking and cough, features a signature waveform (marked by the colored shadows) for easy identification. As expected, the random speaking corresponded to a continuous random current output. Especially noteworthy is that, when the wearer speaks specific words, like “fiber”, “sensor”, “energy”, “generator” and “nanotechnology”, the output current responses exhibit distinct characterized patterns with high repeatability (Fig. S19). This speech-to-text or phonetic recognition may be exploited in speech rehabilitation training and human-machine interaction [63,64]. Wrist pulse is a critically important physiological signal which involves arterial pressure and heartbeat information. Fig. 5g shows the output current of the FNG (attached onto the wrist position) within 5 s before wearing (no load), in relaxation and after exercise. Apparently, the rate and amplitude of the pulse can be acquired readily through the current peaks in real time (Movie S2, Supporting information). This pulse sensing can aid in clinical application, such as detection of hypertension and cardiovascular diseases [65,66]. Collectively, the FNG realizes the effective sensing of vigorous joint-bending and joint-twisting related motions, as well as subtle physiological signals such as respiration, pulse, and speech recognition. To the best of our knowledge, it is the first reported self-powered wearable fiber sensor capable of covering the full-range of human activities, which paves the way for full-range personal healthcare monitoring in a self-powered, wearable and noninvasive manner.

Supplementary material related to this article can be found online at http://dx.doi.org/10.1016/j.nanoen.2017.10.010.

3. Conclusion

In summary, a stretchable FNG with coaxial core-sheath configuration is devised. The FNG is able to harvest multiple mechanical energy, including stretch, bend, twist and press, with a peak output power density of 2.25 nW/cm^2. Simulation of the structural response of the FNG to various mechanical stimuli is implemented to better understand the gap size variation induced energy conversion based on electrostatic effect. The FNG is utilized as wearable sensors, and realizes the detection of joint-bending and joint-twisting related motions, such as walking and elbow rotation, and also succeeds in capturing subtle physiological signals, such as breath, pulse and speech recognition. This wearable FNG holds great potential for full-range personal healthcare monitoring in a self-powered, noninvasive manner.

Acknowledgements

This work is supported by the National Research Foundation Singapore, Ministry of National Development (MND), R-263-000-C22-277. This work is also supported by NUS Hybrid-Integrated Flexible (Stretchable) Electronic Systems Program.

Appendix A. Supplementary material

Supplementary data associated with this article can be found in the online version at http://dx.doi.org/10.1016/j.nanoen.2017.10.010.

References

[1] J.A. Rogers, T. Someya, Y. Huang, Science 327 (2010) 1603–1607.
[2] D.H. Kim, J. Xiao, J. Song, Y. Huang, J.A. Rogers, Adv. Mater. 22 (2010) 2108–2124.
[3] W. Zeng, L. Shu, Q. Li, S. Chen, F. Wang, X.M. Tao, Adv. Mater. 26 (2014) 5310–5336.
[4] H. Wu, Y. Huang, F. Xu, Y. Duan, Z. Yin, Adv. Mater. 28 (2016) 9881–9919.
[5] F.R. Fan, W. Tang, Z.L. Wang, Adv. Mater. 28 (2016) 4283–4305.
[6] J.J. Park, W.J. Hyun, S.C. Mun, Y.T. Park, O.O. Park, ACS Appl. Mater. Interfaces 7 (2015) 6317–6324.
[7] J. Lee, H. Kwon, J. Seo, S. Shin, J.H. Koo, C. Pang, S. Son, J.H. Kim, Y.H. Jang, D.E. Kim, T. Lee, Adv. Mater. 27 (2015) 2433–2439.
[8] S. Jung, J. Lee, T. Hyeon, M. Lee, D.H. Kim, Adv. Mater. 26 (2014) 6329–6334.
[9] C. Choi, J.M. Lee, S.H. Kim, S.J. Kim, J. Di, R.H. Baughman, Nano Lett. 16 (2016) 7677–7684.
[10] S. Ryu, P. Lee, J.B. Chou, R.Z. Xu, R. Zhao, A.J. Hart, S.G. Kim, ACS Nano 9 (2015) 5929–5936.
[11] T. Yamada, Y. Hayamizu, Y. Yamamoto, Y. Yomogida, A. Izadi-Najafabadi, D.N. Futaba, K. Hata, Nat. Nanotechnol. 6 (2011) 296–301.
[12] B.U. Hwang, J.H. Lee, T.Q. Trung, E. Roh, D.I. Kim, S.W. Kim, N.E. Lee, ACS Nano 9 (2015) 8801–8810.
[13] C. Larson, B. Peele, S. Li, S. Robinson, M. Totaro, L. Beccai, B. Mazzolai, R. Shepherd, Science 351 (2016) 1071–1074.
[14] J. Kim, M. Lee, H.J. Shim, R. Ghaffari, H.R. Cho, D. Son, Y.H. Jung, M. Soh, C. Choi, S. Jung, K. Chu, D. Jeon, S.T. Lee, J.H. Kim, S.H. Choi, T. Hyeon, D.H. Kim, Nat. Commun. 5 (2014) 5747.
[15] Y. Cheng, R. Wang, H. Zhai, J. Sun, Nanoscale 9 (2017) 3834–3842.
[16] S. Jung, J.H. Kim, J. Kim, S. Choi, J. Lee, I. Park, T. Hyeon, D.H. Kim, Adv. Mater. 26 (2014) 4825–4830.
[17] S. Lim, D. Son, J. Kim, Y.B. Lee, J.-K. Song, S. Choi, D.J. Lee, J.H. Kim, M. Lee, T. Hyeon, D.-H. Kim, Adv. Funct. Mater. 25 (2015) 375–383.
[18] J.M. Donelan, Q. Li, V. Naing, J.A. Hoffer, D.J. Weber, A.D. Kuo, Science 319 (2008)

807–810.
[19] P. Bai, G. Zhu, Z.-H. Lin, Q. Jing, J. Chen, G. Zhang, J. Ma, Z.L. Wang, ACS Nano 7 (2013) 3713–3719.
[20] Y. Qi, M.C. McAlpine, Energy Environ. Sci. 3 (2010) 1275.
[21] J.H. Lee, K.Y. Lee, M.K. Gupta, T.Y. Kim, D.Y. Lee, J. Oh, C. Ryu, W.J. Yoo, C.Y. Kang, S.J. Yoon, J.B. Yoo, S.W. Kim, Adv. Mater. 26 (2014) 765–769.
[22] M. Lee, C.-Y. Chen, S. Wang, S.N. Cha, Y.J. Park, J.M. Kim, L.-J. Chou, Z.L. Wang, Adv. Mater. 24 (2012) 1759–1764.
[23] C.K. Jeong, J. Lee, S. Han, J. Ryu, G.T. Hwang, D.Y. Park, J.H. Park, S.S. Lee, M. Byun, S.H. Ko, K.J. Lee, Adv. Mater. 27 (2015) 2866–2875.
[24] S.Y. Chung, S. Kim, J.-H. Lee, K. Kim, S.-W. Kim, C.-Y. Kang, S.-J. Yoon, Y.S. Kim, Adv. Mater. 24 (2012) 6022–6027.
[25] T. Huang, C. Wang, H. Yu, H. Wang, Q. Zhang, M. Zhu, Nano Energy 14 (2015) 226–235.
[26] K.N. Kim, J. Chun, J.W. Kim, K.Y. Lee, J.-U. Park, S.-W. Kim, Z.L. Wang, J.M. Baik, ACS Nano 9 (2015) 6394–6400.
[27] W. Seung, M.K. Gupta, K.Y. Lee, K.-S. Shin, J.-H. Lee, T.Y. Kim, S. Kim, J. Lin, J.H. Kim, S.-W. Kim, ACS Nano 9 (2015) 3501–3509.
[28] T. Zhou, C. Zhang, C.B. Han, F.R. Fan, W. Tang, Z.L. Wang, ACS Appl. Mater. Interfaces 6 (2014) 14695–14701.
[29] X. Yu, J. Pan, J. Zhang, H. Sun, S. He, L. Qiu, H. Lou, X. Sun, H. Peng, J. Mater. Chem. A 5 (2017) 6032–6037.
[30] J. Zhong, Y. Zhang, Q. Zhong, Q. Hu, B. Hu, Z.L. Wang, J. Zhou, ACS Nano 8 (2014) 6273–6280.
[31] Q. Zhong, J. Zhong, B. Hu, Q. Hu, J. Zhou, Z.L. Wang, Energy Environ. Sci. 6 (2013) 1779.
[32] X. Yu, J. Pan, J. Deng, J. Zhou, X. Sun, H. Peng, Adv. Mater. 28 (2016) 10744–10749.
[33] S. Li, W. Peng, J. Wang, L. Lin, Y. Zi, G. Zhang, Z.L. Wang, ACS Nano 10 (2016) 7973–7981.
[34] Z. Li, Z.L. Wang, Adv. Mater. 23 (2011) 84–89.
[35] X. Pu, L. Li, M. Liu, C. Jiang, C. Du, Z. Zhao, W. Hu, Z.L. Wang, Adv. Mater. 28 (2016) 98–105.
[36] Y. Zi, L. Lin, J. Wang, S. Wang, J. Chen, X. Fan, P.K. Yang, F. Yi, Z.L. Wang, Adv. Mater. 27 (2015) 2340–2347.
[37] X. Li, Z.-H. Lin, G. Cheng, X. Wen, Y. Liu, S. Niu, Z.L. Wang, ACS Nano 8 (2014) 10674–10681.
[38] J.W. Zhong, H.L. Zhu, Q.Z. Zhong, J.Q. Dai, W.B. Li, S.H. Jang, Y.G. Yao, D. Henderson, Q.Y. Hu, L.B. Hu, J. Zhou, ACS Nano 9 (2015) 7399–7406.
[39] P.K. Yang, L. Lin, F. Yi, X. Li, K.C. Pradel, Y. Zi, C.I. Wu, J.H. He, Y. Zhang, Z.L. Wang, Adv. Mater. 27 (2015) 3817–3824.
[40] Y.-C. Lai, J. Deng, S.L. Zhang, S. Niu, H. Guo, Z.L. Wang, Adv. Funct. Mater. 27 (2017) 1604462.
[41] Z. Zhao, C. Yan, Z. Liu, X. Fu, L.M. Peng, Y. Hu, Z. Zheng, Adv. Mater. 28 (2016) 10267–10274.
[42] Q. Zhong, J. Zhong, X. Cheng, X. Yao, B. Wang, W. Li, N. Wu, K. Liu, B. Hu, J. Zhou, Adv. Mater. 27 (2015) 7130–7136.
[43] J. Zhong, Q. Zhong, G. Chen, B. Hu, S. Zhao, X. Li, N. Wu, W. Li, H. Yu, J. Zhou, Energy Environ. Sci. 9 (2016) 3085–3091.
[44] N. Wu, X. Cheng, Q. Zhong, J. Zhong, W. Li, B. Wang, B. Hu, J. Zhou, Adv. Funct. Mater. 25 (2015) 4788–4794.
[45] X. He, Y. Zi, H. Guo, H. Zheng, Y. Xi, C. Wu, J. Wang, W. Zhang, C. Lu, Z.L. Wang, Adv. Funct. Mater. 27 (2017) 1604378.
[46] J. Zhong, Q. Zhong, Q. Hu, N. Wu, W. Li, B. Wang, B. Hu, J. Zhou, Adv. Funct. Mater. 25 (2015) 1798–1803.
[47] H.J. Sim, C. Choi, S.H. Kim, K.M. Kim, C.J. Lee, Y.T. Kim, X. Lepro, R.H. Baughman, S.J. Kim, Sci. Rep. 6 (2016) 35153.
[48] Y. Wei, S. Chen, X. Yuan, P. Wang, L. Liu, Adv. Funct. Mater. 26 (2016) 5078–5085.
[49] Y. Cheng, R. Wang, J. Sun, L. Gao, ACS Nano 9 (2015) 3887–3895.
[50] Z.F. Liu, S. Fang, F.A. Moura, J.N. Ding, N. Jiang, J. Di, M. Zhang, X. Lepro, D.S. Galvao, C.S. Haines, N.Y. Yuan, S.G. Yin, D.W. Lee, R. Wang, H.Y. Wang, W. Lv, C. Dong, R.C. Zhang, M.J. Chen, Q. Yin, Y.T. Chong, R. Zhang, X. Wang, M.D. Lima, R. Ovalle-Robles, D. Qian, H. Lu, R.H. Baughman, Science 349 (2015) 400–404.
[51] R. Wang, H. Zhai, T. Wang, X. Wang, Y. Cheng, L. Shi, J. Sun, Nano Res. 9 (2016) 2138–2148.
[52] S. Han, S. Hong, J. Ham, J. Yeo, J. Lee, B. Kang, P. Lee, J. Kwon, S.S. Lee, M.Y. Yang, S.H. Ko, Adv. Mater. 26 (2014) 5808–5814.
[53] P. Lee, J. Lee, H. Lee, J. Yeo, S. Hong, K.H. Nam, D. Lee, S.S. Lee, S.H. Ko, Adv. Mater. 24 (2012) 3326–3332.
[54] X. Wang, H. Hu, Y. Shen, X. Zhou, Z. Zheng, Adv. Mater. 23 (2011) 3090–3094.
[55] F. Xu, Y. Zhu, Adv. Mater. 24 (2012) 5117–5122.
[56] C. Yu, C. Masarapu, J. Rong, B. Wei, H. Jiang, Adv. Mater. 21 (2009) 4793–4797.
[57] Y. Suzuki, IEEJ Trans. Electr. Electr. 6 (2011) 101–111.
[58] H. Zheng, N.D. Black, N.D. Harris, Med. Biol. Eng. Comput. 43 (2005) 413–420.
[59] H. Zhou, H. Hu, Biomed. Signal Process. 3 (2008) 1–18.
[60] E. Jovanov, A. Milenkovic, C. Otto, P.C. de Groen, J. Neuroeng. Rehabil. 2 (2005) 6.
[61] J.G. Brooks, Am. J. Dis. Child. 136 (1982) 1012–1023.
[62] V.L. Schechtman, R.M. Harper, K.A. Kluge, A.J. Wilson, H.J. Hoffman, D.P. Southall, Sleep 11 (1988) 413–496.
[63] A. Sears, J. Feng, K. Oseitutu, C.-M. Karat, Hum. Comput. Interact. 18 (2003) 229–257.
[64] M.J. Fagan, S.R. Ell, J.M. Gilbert, E. Sarrazin, P.M. Chapman, Med. Eng. Phys. 30 (2008) 419–425.
[65] J.N. Cohn, S. Finkelstein, G. McVeigh, D. Morgan, L. LeMay, J. Robinson, J. Mock, Hypertension 26 (1995) 503–508.
[66] J. Blacher, R. Asmar, S. Djane, G.M. London, M.E. Safar, Hypertension 33 (1999) 1111–1117.

Cheng Yin received the B.S. degree (2011) in materials science and engineering from North China Electric Power University (Beijing) and the Ph.D. degree (2016) in Materials Physics and Chemistry from Shanghai Institute of Ceramics, Chinese Academy of Sciences (SICCAS). He is now working as a research fellow in National University of Singapore in Ho Ghim Wei's group, focusing on flexible and wearable electronics.

Lu Xin received his Bachelor of Engineering (Mechanical Engineering) with a specialization in Offshore Oil & Gas Technology from the National University of Singapore in 2016. Now he is a Master of Engineering (M.Eng.) candidate under Prof Zeng Kaiyang and Prof Ho Ghim Wei at NUS. His research interests include thin film nanogenerators and application of the Atomic Force Microscope (AFM) in research.

Chan Kwok Hoe has received a B. Eng (Engineering Science, specialization in Nanoscience & Nanotechnology) degree from National University of Singapore in 2014. He worked in developing nanogenerators for harvesting natural renewable energy sources.

Wang Ranran received her B.S. degree (2007) from China University of Petroleum and PhD degree (2012) from SICCAS. She is now working as an associate researcher in SICCAS. Her research interests include controllable synthesis and industrialization of metal nanowires, application of metal nanowires based transparent conductive films, stretchable and wearable electronics.

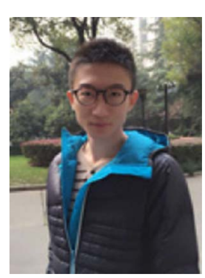

Cao Zherui received his B.S. degree from Liaoning University in 2014 and is now a Ph.D. candidate in SICCAS in Prof. Sun jing's group. His research interests include elastic conducting fibers for electronic textiles.

Sun Jing received her M.S. from Changchun Institute of Applied Chemistry and Ph.D. degree from Shanghai Institute of Ceramics in 1994 and 1997, respectively. Then she joined Shanghai Institute of Ceramics (SICCAS). She spent one year as visiting scientist in Institute for Surface Chemistry in Stockholm (YKI) between 1999 and 2000 and as a JSPS fellow in National Institute of Advanced Science and Technology (AIST) in Japan during 2002–2004. She has been appointed as a Professor in SICCAS since 2005 and now is leading a research group focusing on photo-catalysis for indoors & outdoors air-cleaning and flexible electronics.

Ho Ghim Wei graduated with a B.Sc. and M.Sc. from the National University of Singapore in 2000. She worked as an Engineer at Chartered Semiconductor Manufacturing (CSM), Singapore from 2000 to 2002, before embarking her Ph.D. at the University of Cambridge. She was elected a Scholar at Selwyn College, University of Cambridge in 2003. Upon completion of her Ph.D. in 2006, she worked as a postdoctoral researcher at University of Cambridge and subsequently joined NUS. She is currently an Associate Professor of the Department of Electrical & Computer Engineering at the National University of Singapore (NUS). She is also one of the pioneer faculty associates of the Engineering Science Programme (ESP) at NUS.